

# Clearing-up channel in contrails

A.N. Kucherov

*N.E. Zhukovskii Central Institute for Aerohydrodynamics, Moscow*

Received March 15, 2000

This paper gives a brief review of the investigations into the gas dynamics, physicochemical, and optical properties of the contrails behind high-altitude airplanes. In addition, a possibility is assessed of clearing up the exhaust wake with a laser beam to facilitate remote sensing its near-axis region with the highest concentration of contaminating effluents.

## Introduction

In recent years there is observed an increased interest in studies of the atmospheric emissions from aircraft and their influence on the atmosphere.<sup>1-9</sup> The studies of the appearance and evolution of the contrails (condensation trails behind aircraft) are closely related to the studies of atmospheric pollution and, in particular, to the problem of the influence of the atmospheric emissions from aircraft on the atmospheric ozone.<sup>10</sup> According to ICAO information<sup>4</sup> (International Civil Aviation Organization), the air transportation has been steadily increasing, at the annual-mean rate of 5-6%, in the years from 1970 to 1993, and 7 to 8%, in 1994 to 1996. The amount of fuel burnt during the period from 1992 to 1995 totals about 1.3 to 1.8 by  $10^{14}$  g/year that makes about 6% of all oil products. About 65%, of that amount of fuel has been mostly burnt in wide-body aircraft, like Boeing-747, while cruising at altitudes from 10 to 13 km in the latitude belt between 30°N and 55°N over the USA, Europe, and the North Atlantic. About 34% of the fuel is burnt at the altitudes above the tropopause. The fraction of fuel burnt in the stratosphere above the North Atlantic reaches 50%. The annual growth of the fuel consumption in aviation reached 3% during the past 20 years. The altitude of cruising for supersonic carriers of the second generation (SGC-2) will be about 15 to 18 km at Mach number M about 2 (like the Concorde aircraft) or 18 to 20 km at M about 2.4 (see Ref. 2). These altitudes are already near the level of the ozone maximum (~24 km) and of the polar stratospheric clouds (~20 km).

## 1. Contaminating emissions

The emissions of exhaust gases from aircraft engines have been studied in flights and in ground-based model experiments.<sup>5-8</sup> Burning of one kilogram of fuel (kerosene) yields 3.15 kg of CO<sub>2</sub> and 1.25 kg H<sub>2</sub>O (see Refs. 2-4). One kilogram of kerosene used in aviation can contain from 0.001 g to 3 g of sulfur. In the process of combustion, the sulfur mainly transforms into SO<sub>2</sub> (also into SO<sub>3</sub> and into the sulfur acid

H<sub>2</sub>SO<sub>4</sub>). The mean content of sulfur in the fuel ranges from 0.4 to 0.5 gram per kilo. The emission index for SO<sub>2</sub>, that is, its mass emitted per unit mass of the fuel burnt, is from 0.8 to 1.0 g/kg.

Depending on the environmental conditions, type and power of the aircraft engine the combustion of fuel can yield 7 to 30 grams of nitrogen oxides (in units of NO<sub>2</sub> mass) per kilogram of the burnt fuel. The mean, over different types of aircraft, emission of NO<sub>2</sub> is 13 to 15 g/kg. Predictions show that omissions of nitrogen oxides (NO<sub>x</sub>) from the SGC<sub>s</sub> will cause a significant depletion of the ozone.<sup>1</sup> Early predictions assessed the emission of NO<sub>x</sub> from the aircraft engines to be at the level of 30 grams per one kilo of the burnt fuel.<sup>1</sup> Later on, the level of 5 g/kg of NO<sub>x</sub> emission was achieved in the experiments with the combustion chambers of practicable configurations. Contemporary models of the atmosphere show that at that low level of the NO<sub>x</sub> emission the technology of SGC-based aviation can be quite friendly to the environment.<sup>6</sup>

Modern aircraft engine also emits about 0.01 to 0.1 gram of soot per kilogram of the burnt fuel.<sup>1-4</sup> Typical diameter of soot particles is from 10 to 30 nm. The number of soot particles per one kilogram of burnt fuel was recorded in observations to be at the level of  $10^{15}$ . The emission of CO and CHO normally decreases with the increasing power of an engine. Typical measured values of the emission index are from 1 to 10 g/kg for CO and 0.1 to 1.0 for the CHO. The exhaust gases emitted from the engines also contain charged particles that are produced during the combustion process. These charged particles are apt to coagulate at a higher rate compared to uncharged particles thus accelerating formation of large particles in the exhaust trail behind the aircraft. The particles of soot and charged particles can serve the centers of condensation and crystallization thus yielding aerosol particles. The condensation of water and freezing of (droplets of liquid solutions, behind airplanes at high altitudes, contribute to formation of the visible condensation trails (contrails) that evolve and transform into the aerosol formations similar to natural cirrus clouds. The contrails transformed into stable formations can affect the ozone layer, the radiative balance, and, in particular, they may result in an

increase of the Earth's surface temperature. To provide for remotely sensing the inside of the contrails, one has to be able to create the clearing-up channel in it, for example, by use of a laser beam.<sup>11-15</sup>

## 2. Structure of the exhaust trail

Three stages are normally isolated in the evolution of the exhaust trails, namely, the jet-stream stage, vortex stage, and the stage of the trail dispersion.<sup>16-19</sup> Then the long diffusion process completes the trail emission mixing with the ambient air.<sup>20,21</sup> In Refs. 17, 22, and 23 one can find a rigorous numerical model of contrails at the jet-stream stage, and approximate models are considered in Refs. 23-26. At this stage, the hot gases emitted from the engine nozzle freely expand behind the aircraft. The vortex sheet that appears around the wings rolls up, by approximately the tips of wings, into two vortices rotating, during the flight, in counter directions. The jet-stream stage lasts approximately 10 seconds for the wide-body aircraft of Boeing-747-400 type.<sup>20,24</sup>

The vortex stage involves an early stage of the vortex wake evolution and its interaction with the exhaust jet stream.<sup>18,19,21,27-29</sup> To describe the passage from the aircraft trail formed due to interaction between the pair of wake vortices and the exhaust stream, affected by the Archimedes force, to the trail

formed due to dispersion in the atmosphere the model of large vortices (MLV) was used in Refs. 18, 19, and 21. At the vortex stage the pair of vortices descends under due to mutual velocity induction. Most of the exhaust gases retain in this primary trail so they also descend below the flight altitude. However, part of the exhaust gases is entrained by the secondary wake, which is formed by the vortices themselves. The secondary trail ties up the vortices to the flight altitude.<sup>21</sup> Duration of the vortex stage is usually about 2 minutes (see Refs. 20 and 21) or 100 s according to Ref. 24.

Table 1 gives some data for a subsonic Boeing-747-400 aircraft and for a version of supersonic aircraft of the HSCT (High Speed Civil Transport) type.<sup>24,30</sup>

After break up of the vortices the positive buoyancy of the emission jet caused by hot exhaust gases and reduced vorticity of two wakes caused, in turn, by stratification of the ambient medium will dominate until an essential mixing is reached of the exhaust gases with the ambient air. Normally this dispersion stage lasts about 10 minutes<sup>20,21</sup> or 1000 s according to Ref. 24.

Finally, in a later time, the diffusion of the exhaust emission is governed by its interaction with the ambient air due to atmospheric turbulence, gravitational waves, and shear gradients.<sup>27</sup>

**Table 1. The altitudes, Mach number in cruise, temperatures at the exit nozzle and mole fractions of water vapor H<sub>2</sub>O and nitrogen dioxide NO<sub>2</sub>, transient times for jet-vortex and vortex-dispersion stages for a Boeing-747-400 and HSCT aircraft<sup>24,30</sup>**

Aircraft	<i>h</i> , km	<i>T</i> , K	Mach number	C <sub>H<sub>2</sub>O</sub>	C <sub>NO<sub>2</sub></sub>	<i>t</i> , s (jet)	<i>t</i> , s (vortex)
Boeing-747-400	10.6	590	0.8	4.28 · 10 <sup>-2</sup>	2.25 · 10 <sup>-5</sup>	8	66
HSCT	18.4	561	2.4	3.02 · 10 <sup>-2</sup>	4.80 · 10 <sup>-6</sup>	0.2	31

**Table 2. The initial data for use in modeling by MLV method**

Version No.	1	2	3	4
Aircraft	Boeing-737	ER-2	Boeing-737	Boeing-737
Wing span, m	28.9	31.4	60.8	60.8
Speed of air, m/s	244	201	268	26
Engines	2 on wings	1 in the tail	4 on wings	4 on wings
$\int Tdydz, j \cdot m^2$	1100	430	8600	8600
Distance between wakes, m	22.7	23.9	47.4	47.7
Vortex's core radius, m	2.5	5.0	4.6	4.6
Circulation, m <sup>2</sup> /s	220	383	414	414
<i>t<sub>f</sub></i> , s	14.7	9.4	34.1	34.1
Atmospheric parameters				
$N = (g/\rho) d\rho/dz, s^{-1}$	0.012	0.021	0.012	0.012
Shear $S = du/dz, s^{-1}$	0	0	0	0.02
TKE, m <sup>2</sup> /s (turbulent, kinetic energy)	0.1	0.05	0.09	0.07
Numerical modeling parameters				
Grid domain, km	0.2×0.24×0.32	0.2×0.24×0.32	0.4×1×1	0.2×1×0.8
Minimal cell, m	2×1×1	2×1.1×1.1	4×2×2	2×2×2

**Table 3. The exhaust parameters at different stages of its evolution**

Parameter	Jet		Vortex			Dispersion		Diffusion	
	1 s	20 s	20 s	80 s	130 s	130 s	5 min	1 h	10 h
$D_h, m^2/s$	0.4	0.4	–	0	–	0.1	2...20	14...23	
$D_v, m^2/s$	0.4	0.4	–	30	–	0	$\leq 0$	0.15...0.18	
$c_{pri}/c_0, 10^{-4}$	300	2...3	–	1...2	–	0.3...1	0.2	0.001	$\leq 0.001$
$c_{sec}/c_0, 10^{-4}$	–	–	–	0.6...0.2	–	0.1...0.3	0.4		
$A_{pri}, 10^{-4} m^2$	0.05	0.3...0.4	–	0.5...0.9	–	0.5...2	5	20...50	$10^2...>10^3$
$A_{sec}, 10^{-4} m^2$	–	–	–	0.08...0.8	–	0.5...2	2		
$w, 10^{-3} s^{-1}$	800	3...5	–	3...30	–	30...40	2	0.1...0.3	

Note: Table gives typical data on diffusion, dilution, and mixing of the emissions from a subsonic wide-body aircraft under stable stratified atmosphere at heights of aircraft cruising.  $D_h$   $D_v$  are horizontal and vertical diffusion coefficients;  $c/c_0$  is dilution measure of the exhaust (averaged along a flight) for primary (pri) and secondary (sec) wake,  $c_0$  is the concentration at the nozzle exit;  $A$  is the cross section of the exhaust (at  $10^{-7}$  level of the mean concentration  $c_0$ );  $w$  is entrainment rate  $w = -d(\ln[c_{max}])/dt$  (normalized to maximum  $c$ ). The ranges of values at the diffusion stage for thermal stratification  $N$  are between 0.011 and 0.023  $s^{-1}$ , for wind shear  $S$  between 0 and 0.007  $s^{-1}$ , turbulence is assumed to be weak; for all other regimes  $N = 0.014 s^{-1}$  and  $S = 0$ .

The early stage of the vortex mode has been studied numerically for a 2D case,<sup>29</sup> with the account for atmospheric disturbances, stratification, buoyancy, and shear gradients. A 3D explicit modeling of nonstationary decay of the mutually inductive vortex wake behind an aircraft can be found in Ref. 21. The latter study aimed at elucidating the effects of the dynamics and chemistry in the mixing processes that take place in the wake. The boundary conditions used in that modeling were the results of modeling the near-distance wakes behind Boeing-737, Boeing-747, and ER-2 aircraft. Table 2 gives some data calculated for different aircraft, atmospheric conditions, and parameters of numerical models used in four situations. The initial distance between the wakes,  $b_0$ , radius of the wake core,  $r_0$ , circulation,  $c$ , and the initial fall time,  $t_f$ , (defined as the initial distance  $b_0$  divided by the initial speed of the wake ascend) are approximate data calculated by use of the UNIWAKE computer code.<sup>31</sup>

The contrail dispersal on longer time scales that takes place due to the dynamics of the atmosphere has been studied in several recent papers, including those, which use the method of large vortices.<sup>27</sup>

The duration of different stages and the diffusion coefficients that determine the evolution of the contrail are given in Table 3.<sup>18,20</sup>

Results of modeling the evolution of interaction between the wakes and the exhaust emission jet have been compared with the photos<sup>21</sup> and experimental data obtained with lidars.<sup>27</sup>

### 3. Criterion of the contrail formation

Under favorable conditions in the atmosphere, (a proper combination of the moisture content, temperature, and pressure) a visible condensation trail is being formed in the exhaust jet comprising water droplets and ice crystals. The evolution of a contrail is closely related to the physicochemical transformations of the exhaust emission. The process of contrail formation itself, the distance from the engine nozzle to the condensation (crystallization) surface, as well as

the initial water and ice content do determine further evolution of the emitted contaminations. Let us derive, based on results from Refs. 2–5 and following the approach proposed in Ref. 6, the conditions of condensation in the contrail. In so doing we take the pressure in the exhaust jet to be equal to pressure in ambient atmosphere,  $p \cong p_\infty$ . One kilogram of burnt fuel adds  $E_w$  kg of water vapor to the atmosphere ( $E_w$  is the water emission index),  $(1 - \eta) \epsilon_f$  J of heat energy from the engine and  $q/q_f$  kg of the exhaust gases (primarily this is the air). Here  $\epsilon_f$  is the specific heating capacity of the fuel;  $\eta = A/Q$  is the engine efficiency;  $A = Fu_\infty$  is the useful power;  $F$  is the jet thrust;  $u_\infty$  is the speed of aircraft;  $Q = \epsilon_f q_f$  is the full power of the engine;  $q_f$  and  $q$  are the fuel burn-up and the full consumption of gases. Mixing the exhaust gases with  $N$  parts of ambient air (being at temperature  $T_\infty$ ) yields a temperature increase of the mixture that can be obtained from the following equation:

$$(1 - \eta) q_f \epsilon_f + (1 + N) q Y_L L = (1 + N) q C_p (T - T_\infty)$$

or

$$T - T_\infty = \frac{(1 - \eta) \epsilon_f q_f}{q(1 + N) C_p} + \frac{Y_L L}{C_p}. \tag{1}$$

Here  $C_p$  is the specific heat of the mixture at a constant pressure;  $L(T)$  is the specific heat of water vapor condensation;  $Y_L = \rho_L/\rho$  is the mass concentration of the condensed water. Let us also introduce the mass concentration of water vapor in the mixture  $Y = \rho_v/\rho$ , where  $\rho_v$ , and  $\rho_L$ ,  $\rho$  are the density of water vapor, liquid water, and of the mixture. Note that  $q = \rho u_\infty$ .

Write down now the equation of water mass conservation during the condensation for the mixture of  $(1 + N)q$  mass. The air entering the engine per unit of time contains  $(q - q_f) Y_\infty \approx q Y_\infty$  mass of water vapor. The fuel combustion and mixing in of air add  $E_w q_f$  and  $Nq Y_\infty$  water vapor more. Condensation transforms a portion of water vapor into liquid water whose mass equals  $(1 + N) q Y_L$ . Concentration of the rest water vapor is  $Y_{sw}(T) \cong \mu_w p_{sw}(T)/\mu p_\infty$ , where  $p_{sw}(T)$  is the saturation water vapor pressure above the water

surface at the temperature of the mixture  $T$ ;  $\mu_w$ ,  $\mu$  are the molar masses of water and the gas mixture (air). The equation of the water (liquid and vapor) mass conservation is as follows:

$$(1 + N) q Y_\infty + E_w q_f = (1 + N) q Y_{sw}(T) + (1 + N) q Y_L(T). \quad (2)$$

By substituting  $q_f/(1 + N) q$  from expression (1) we have

$$Y_{sw}(T) - Y_\infty = C(T - T_\infty) - Y_L(T) \left[ 1 + \frac{E_w L}{(1 - \eta) \varepsilon_f} \right];$$

$$C = \frac{E_w C_p}{(1 - \eta) \varepsilon_f} \cong \text{const}. \quad (3)$$

At the condensation threshold the value  $Y_L = 0$  and according to Ref. 32 one obtains the known relationship

$$\Delta Y \equiv Y_{sw}(T_c) - Y_\infty = C(T_c - T_\infty) \equiv C \Delta T. \quad (4)$$

The left-hand side of the equation (4) is an exponential curve as a function of  $T$  while the right-hand side being the straight line. If these two curves do not cross each other, no condensation occurs. In case of condensation, the two curves do cross each other twice, in the general case. Between the cross points (temperatures) that correspond to the beginning and end of the condensation trail, water vapor is supersaturated and partially condensed into liquid water. At the condensation threshold liquid water content equals zero and the straight line contacts the exponential curve at a single point  $T = T_c$ . The criterion of condensation is expressed through the following two conditions  $Y_L = 0$ ,  $dY_L/dT = 0$  that must be fulfilled simultaneously, or, according to Eq. (3), one has the following form for this criterion

$$\frac{dY_{sw}(T_c)}{dT} = C. \quad (5)$$

By making use of the Clausius-Clapeyron equation

$$p_{sw}(T) = p_{sw}(T_\infty) \exp \left[ \int_{T_\infty}^T \frac{\mu_w L(T)}{RT^2} dT \right],$$

one can calculate the derivative  $dY_{sw}/dT = Y_{sw}(T_c) \mu_w L(T_c)/RT_c^2$  and then find from Eqs. (4) and (5) that at the condensation threshold a small temperature increase,  $\Delta T = (T_c - T_\infty)$ , can be presented by the following expression:

$$\frac{\Delta T}{T_\infty} \cong \frac{RT_\infty}{\mu_w L_\infty} - \frac{Y_\infty}{CT_\infty} + \frac{RT_\infty}{\mu_w L_\infty} \left( \frac{RT_\infty}{\mu_w L_\infty} - \frac{Y_\infty}{CT_\infty} \right) \left( 2 - \frac{T_\infty}{L_\infty} \frac{dL(T_\infty)}{dT} \right). \quad (6)$$

The last term in this sum can be neglected since its relative contribution to the threshold temperature of condensation amounts to thousandths even at  $Y_\infty = 0$  (dry air). Substituting the threshold temperature  $T_c$  in Eq. (4) yields the threshold value of the ambient pressure  $p_{xc}$ , above which the condensation occurs

given the temperature of the ambient air  $T_\infty$  and the water vapor content  $Y_\infty$

$$p_{xc} = \frac{\mu_w p_{sw}(T_\infty + \Delta T)}{\mu C \Delta T + Y_\infty}. \quad (7)$$

The equation (7) can also be used for determining the threshold temperature of ambient air,  $T_{xc}$ , below which the water vapor condensation is possible at some height of flight (pressure  $p_x$ ) and water vapor content (relative humidity of the ambient air  $S_\infty = \rho_{v\infty}/\rho_{sw\infty} = Y_\infty/Y_{sw\infty}$ , where  $\rho_{sw\infty}$  and  $Y_{sw\infty}$  are the density and mass concentration of water vapor saturated above the water surface;  $\rho_{v\infty}$  is the water vapor density at the temperature  $T_\infty$ ). It is worthy to note that in an absolutely dry air ( $Y_\infty = 0$ ) the increase of temperature of the mixture near the point of trail condensation threshold does not depend on the parameters of fuel and the engine (the constant  $q$ ) being only determined by the atmospheric temperature  $T_\infty$ . However, some details of the contrail formation process, like composition of aerosol particles, phase state, and concentration of individual components are still unclear<sup>37</sup>.

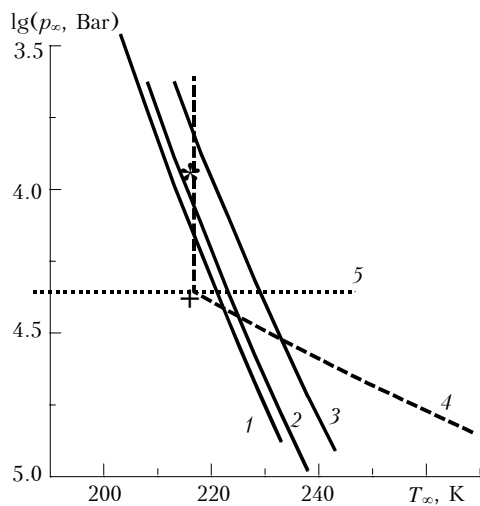
In Ref. 32 it was noted for the first time the constant ratio between the increase of the vapor concentration and temperature increase in the contrail,  $\Delta Y/\Delta T \cong dY/dT = q$  (see Eqs. (4) and (5)). The study presented in Ref. 34 was stated the necessity of taking into account the engine efficiency. The study in Ref. 35 was the first to introduce into consideration the concentration  $Y_L$  of liquid water in making rigorous analysis of the process. It is worth noting that the expressions derived in Ref. 35 are incorrect since these were obtained by use of asymptotic series expansion of the expression for the saturation pressure of water vapor over small temperature increase. The matter is that the quantity  $\Delta T/T_\infty \ll 1$ , being on the order of  $RT_\infty/\mu_w L_\infty$  (see Eq. (6) and the power of the exponent in the Clausius-Clapeyron is close to unity, so that its expansion into a series is incorrect. The pressure  $p_{xc}$  calculated in Ref. 35 (page 134) differs from that calculated by formula (7) at  $T_\infty$  from 203 to 273 K and  $S_\infty = 0$  by 10.3 to 8.1%. Increasing  $S_\infty$  results in a decrease in  $\Delta T/T_\infty$  and in the error of calculating  $p_{xc}$  by the formula from Ref. 35 down to 7.4–5.1% at  $S_\infty = 0.5$  and to 2.3–3.3% at  $S_\infty = 1$ .

Let us now give examples of calculating the condensation threshold in the contrails of IL-86 and IL-96 airbuses cruising at 11 km altitude as well as for the Russian supersonic airliner of the second generation<sup>38</sup> cruising at 18 km altitude. In so doing we assume some parameters to have the following values:  $E_w = 1.25$ ;  $\varepsilon_f = 43$  MJ/kg;  $\eta = 0.3$ ;  $T_\infty = 216.7$  K;  $L_\infty = 2.65$  MJ/kg;  $C_p = 1006$  J/(kg · j). The boundaries of the regions for contrail formation are shown in Figure 1. Curve 1 in the figure corresponds to the relative humidity  $S_\infty = 0$ , curve 2 –  $S_\infty = 0.5$ , curve 3 –  $S_\infty = 1.0$ , curve 4

presents the standard atmosphere; + sign denotes data calculated for IL-86 and IL-96 aircraft and asterisk \* for the Russian supersonic airliner of the second generation; the segment of dotted straight line 5 shows the interval of seasonal and latitudinal variation of temperature ( $\pm 30$  °C). At  $T_\infty = 216.7$  j (the conditions at cruising of the aircraft considered) the increase of the mixture temperature at the condensation threshold  $\Delta T = 8.45 - 1.11$  j ( $S_\infty = 0 - 1.00$ ). Homogeneous or heterogeneous (on soot particles) freezing of droplets of pure water or solutions of acids will result in a partial heat release and lead to a decrease in the vapor concentration down to the saturation pressure over ice surface  $p_{si}(T_i) < p_{sw}(T_c)$ . Temperature increase  $\Delta T_i = (T_i - T_\infty)$  and concentration of the ice aerosol  $Y_i$  formed can be found in a similar way by use of the equation of energy and mass conservation. Thus, one obtains

$$\frac{\Delta T_i}{T_\infty} \cong \frac{\Delta T}{T_\infty} + \frac{RT_\infty C}{\mu_w C_p} \frac{L_{i\infty} - L_\infty}{L_\infty} \cong \frac{\Delta T}{T_\infty}, \quad (8)$$

$$Y_i(T_i) = Y_{sw}(T_c) - Y_{si}(T_i) \cong Y_{sw}(T_c) - Y_{si}(T_c). \quad (9)$$



The difference between the crystallization  $T_i$  and condensation  $T_c$  temperatures is negligible. Mass concentration of crystal aerosol  $Y_i$  at  $S_\infty = 0$ , near the low and upper thresholds of condensation ( $T = 222.25$  K;  $p_{\infty c} \approx 0.259$  Bar,  $h \approx 10$  km and  $T_\infty = 216.7$  j ;  $p_{\infty c} \approx 0.147$  Bar,  $h \approx 14$  km), is  $1.27 \cdot 10^{-4}$  and  $1.32 \cdot 10^{-4}$ , respectively; the water ice content

$\rho_i = \rho Y_i \approx 5 \cdot 10^{-5}$  and  $3 \cdot 10^{-5}$  kg/m<sup>3</sup>, so this quite a visible contrail.<sup>32</sup>

### 4. Parameters of the contrails

Parameters of the exhaust gases at the nozzle of jet engines of Boeing-747-400, HST, IL-86, IL-96, and SST-2 can be found correspondingly in Refs. 24, 30, 36, and 38. Note that the strongest cooling and retardation of the exhaust gases occur at the jet stream stage. In Refs. 14, 15, and 36, using approximate analytical<sup>23,24</sup> and semi-empirical formulas<sup>39</sup> for calculating parameters of the exhaust gases at the jet stream stage such initial parameters of the contrail as distances to the condensation and crystallization surfaces, temperature of the gas mixture, excess speed, initial water and water ice content have been calculated. Results calculated by different approximate formulas<sup>12,17,23</sup> have been compared. The differences between the results compared were from 1 to 10% for distances of 1000 m.

In Ref. 36 it was established that relatively small, on the order of 10%, variations in the magnitude of the initial parameters (temperature and humidity), as well as in the atmospheric temperature, caused by change of season (winter or summer) or latitudinal zone (equator, midlatitudes, polar cap) can cause a manifold change (> 100%) of the distance to contrail, its water and ice content, and optical thickness  $\tau$ .

Contrails have the shape of a tube or a stocking with the gradually increasing thickness of the walls. The walls close up at some distance from the aircraft. As shown in Ref. 15 all contrails behind the aircraft have maximum optical thickness in the transverse direction at the section where the walls of the contrail tube close up at the jet axis.

Table 4 borrowed from Ref. 15 lists the following parameters of the contrail: coordinates  $x_{max}$  of the cross sections where the transverse optical thickness reaches its maximum,  $\tau_{max}$ , and its values; the length of the exponential attenuation of radiation  $L_{exp} = 1/bw(x_{max}, 0)$  on the jet axis; ice content of the aerosol,  $w(x_{max}, 0)$ , the excess velocity of the jet  $V = u(x_{max}, 0) - u_\infty$ ; radius of the jet  $R_j$ , and temperature of the exhaust gas  $T(x_{max}, 0)$ . The extinction coefficient of a water ice crystal aerosol for radiation is  $b \cong b_{ext} = 1.7b_i$ . The radiation wavelength taken in calculating extinction is  $10.6 \mu m$  ( $b_i \approx 80$  m<sup>2</sup>/kg is the specific absorption coefficient of ice),  $S_w = 0$ .

**Table 4. The initial parameters of contrails behind Boeing-747, IL-56, IL-96, SST-2, and HSCT aircraft, according to Ref. 15**

Aircraft	Boeing-747[	IL-86	IL-96	SST-2	HSCT*)
Distance $x_{max}$ , m	292	96	40	651	2341
Maximum transverse optical thickness $\tau_{max}$	0.36	0.085	0.154	0.0716	0.0626
The length of exponential attenuation $L_{exp}$ , m	12.99	25.01	12.83	78.73	184.7
Ice content $w(x_{max}, 0)$ , kg/m <sup>3</sup>	$5.66 \cdot 10^{-4}$	$2.94 \cdot 10^{-4}$	$5.73 \cdot 10^{-4}$	$9.34 \cdot 10^{-5}$	$3.98 \cdot 10^{-5}$
Excess velocity $V = u - u_\infty$ , m/s	18.01	26.37	100.6	21.45	5.057
Jet radius $R_j$ , m	4.181	1.91	1.91	4.152	6.25
Temperature $T$ , j	248.1	241.4	248.0	230.8	223.4

\*) Relative humidity  $S_\infty = 0.9$ .

## 5. Clearing up channel in the contrail

The water and ice crystal aerosol of the contrail hampers optical sensing of the interior of the exhaust jet where contaminating components of the emission and the products of chemical reactions are contained. A possibility of creating a channel of reduced optical thickness in a contrail by use of a laser beam capable of evaporating aerosol particles. The grounds for this study are the investigations into clearing up the water-drop clouds.<sup>40-45</sup> Preliminary estimates of the laser beam parameters needed have been calculated in Ref. 11. The interaction of the beam with the aerosol is described, in the water content approximation, by nonlinear Fresnel (or Schrodinger) equation in combination with the equations of aerosol transport and heating of the medium. This problem has the following parameters of similarity: the Fresnel number

$F = 2\pi r_0^2 / \lambda L$ , where  $r_0$  is the beam radius,  $L$  is the path length; parameters of the molecular absorption  $N_g = \alpha_g L$  and of aerosol extinction of radiation  $N_b = w_* b L$ ,  $w_*$  is the characteristic water (ice) content of aerosol,  $\alpha_g$  and  $\alpha_b = w_* b$  are the coefficient of absorption by gases and the aerosol extinction coefficient; the parameter of thermal self-action  $N = (L/r_0)^2 Q(n_0 - 1)/n_0$ ,  $Q = \alpha_* I_0 t_0 / \rho_0 C_p T_0$  is the heating parameter,  $\alpha_* = \max\{\alpha_g, \alpha_a\}$  is the effective absorption coefficient,  $\alpha_a$  is the aerosol absorption coefficient,  $I_0 = P_0 / \pi r_0^2$  is the radiation intensity,  $P_0$  is the beam power,  $t_0 = r_0 / V_0$  is the characteristic time of blowing the beam,  $V_0$  is the excess velocity of the jet stream,  $\rho_0$ ,  $T_0$ ,  $n_0$ ,  $C_p$  are the density, temperature, air refractive index, and the heat capacity at constant pressure; parameter describing the clearing up of aerosol  $N_v = \beta b_a I_0 t_0 / H_0 V_0$ ,  $b_a = \alpha_a / w_*$  is the specific absorption coefficient of aerosol,  $\beta$  denotes the fraction of absorbed energy spent for particle vaporization,  $H_0$  is the latent heat of vaporization of water (ice). In the problem we consider here the clearing up parameter is the basic one. A description of methods for solving the equation of paraxial optics can be found, for instance, in Refs. 46 and 47. A comparison of different calculation algorithms has been done in Ref. 48. Calculations widely use the expansion into Fourier series with the application of fast Fourier transform technique. Normally, at least the second order of equation approximation is used for all independent arguments. It was established for the promising supersonic aircraft SST and HSCT that at the beam radius of 1 to 5 cm and at the distance from the engine nozzle of 1 to 1.5 km (the contrail width about 10 to 40 m) the energy of several hundreds of joules would suffice for achieving an essential reduction of the contrail optical thickness within a channel having several beam's radii width for 1 to 10 ms. In this case the thermal blooming ( $N \leq 10^{-3}$ ), absorption of light by gases ( $N_g \leq 10^{-4}$ ), and the aerosol extinction ( $N_b \leq 10^{-2}$ ) are low enough. The diffraction beam

divergence starts to play an essential role at  $r_0 < 1$  cm. In Ref. 11 the jet parameters were set based on approximate analytical solutions. In Ref. 12, the initial data for the problem on clearing up the contrail were the distribution of parameters obtained using a more rigorous numerical model. Allowing for the particle coagulation yields an essential growth of particle size. It was also established that the vaporization efficiency of an individual particle  $p$  and the similarity parameters  $N$  and  $N_v$  (vaporization and self-action parameter) dependent on it show strong effect on the process. It was shown that at high altitudes and low temperatures the conditions can take place that relatively small changes of the droplet radius due to, for instance, the vaporization under the action of laser radiation can lead to an essential decrease of the vaporization efficiency  $\beta$ .

Vaporization of a particle with the radius  $a$  is described by the following system of equations

$$\frac{da}{dt} = -\frac{j}{\rho_w}; \quad \rho_w C_{pw} \frac{dT}{dt} = \alpha_d I - \frac{3}{a} \{jH + j_T\} \approx 0,$$

where  $\rho_w$ ,  $C_{pw}$ , and  $H$  are the density, specific heat, and the heat of vaporization of water;  $T$  is the temperature of the droplet;  $I$  is the radiation intensity;  $K_a(a)$  and  $\alpha_d = 3K_a/4a$  are the absorption efficiency factor and the volume-mean absorption coefficient of an individual droplet;  $j$  and  $j_T$  are the densities of the mass and heat fluxes from a water drop. Calculating  $j$  and  $j_T$  is described in Ref. 49. By use of the relations of mass and heat fluxes to other parameters one can derive the quantities like  $\beta = jH/\alpha_d I_0 \approx jH/(jH + j_T)$ ,  $N_v$ , and  $N$  as functions of physical parameters of the beam,  $I_0$  and  $r_0$ , as well as of the medium and the droplet. It was shown that the dependences of water content and optical thickness on the clearing up parameter  $N_v$  and on the beam power  $P_0$  (at  $N_v = \text{const}$ ) are essentially different. In that case, the question arises on the correctness of the water content approach used, which assumes the vaporization rate of a particle and the mass flux from its surface to be linear functions of the beam intensity (power). It also assumes that the parameter  $\beta$  is constant. As shown in the study<sup>13</sup> of the clearing up process carried out in a more rigorous formulation allowing for particle size distribution and the decrease of the particle size at vaporization, the water content approach gives quite good results (accurate to within some percent) near the boundary conditions for the diffusion regime of particle vaporization at the modal radius of particles  $a_m < 1.5 \mu\text{m}$  ( $I_0 = 10^7 \text{ W/m}^2$ ), as well as at  $I_0 < 5 \cdot 10^6 \text{ W/m}^2$  ( $a_m = 2.5 \mu\text{m}$ ). Outside these boundaries the approach of water content overestimates the width and depth of the cleared up channel.

In the case of a laser beam propagating across the contrail there is a surface on which the aerosol is formed what results in the appearance of the source term in the aerooptics equations. In Ref. 14 analytical solutions have been obtained for the intensity, water content, and optical thickness of the aerosol similar to

those obtained by Glickler.<sup>50</sup> As an example, case studies have been carried out in this paper on the formation of contrails behind the American HSCT and Russian SST-2 supersonic aircraft as well as subsonic Boeing-747-400, IL-86, and IL-96 airbuses. The above-mentioned parameters have been studied, in Ref. 14, as functions of spatial coordinate and time at the distances of a significant clearing up and of an essential attenuation of radiation.

At high altitudes the water aerosol of clouds and contrails contains water ice crystals.<sup>51</sup> The task of clearing up crystal aerosol incorporates the stage of heating, sublimation, vaporization, and destruction of particles. In Ref. 52 the heat sources that appear inside particles of three habits (flat discs, needles, and spheres) due to absorption of laser radiation have been considered and versatile expressions obtained for estimating the heat and mass fluxes from the surface of particles having different radii.

In Ref. 15 the clearing up of crystal aerosol with the laser beam has been studied based on the water content approach. The versions of the task of clearing up a homogeneous medium (cloud) and the axially symmetric exhaust jet were analyzed. In calculating optical thickness the size distribution of particles and particles' shapes (flat discs, needles, and spheres) were taken into account. The case study included calculations for the contrails behind subsonic aircraft of Boeing-747-400, IL-86, and IL-96 types as well as for the supersonic HSCT and SST-2 aircraft. The shape of particles can affect the absorption, scattering, and extinction of radiation.<sup>53</sup> It was established in this study that, in the infrared region the radiation at 10.6  $\mu\text{m}$  wavelength suits the task of clearing up best of all because of the maximum absorption coefficient. Time of establishing the optical thickness  $\nu$  of the ice aerosol under clearing up is from 3 to 4  $t_0$ . The decrease of optical thickness achievable is larger in contrails as compared to that in homogeneous clouds, at the equivalent initial optical thickness. A manifold increase of the transverse blowing of the jet (by 8 times) results in a twofold decrease of the contrail optical thickness  $\tau$  (IL-86). The clearing up becomes inefficient at the laser beam incidence angles close to the jet axis ( $< 10^\circ$ ) because of sharp increase in  $\tau$ .

Clearing up of crystal aerosol depends on the shape and size of crystals. In the case of flat discs tripling of their thickness leads to doubling of the characteristic clearing up intensity  $\beta I_0$ . For cylinders, an order of magnitude increase of their radius leads to doubling of the characteristic clearing up intensity. In the case of large spheres (mono- anti polydisperse aerosol) a 1.5 to 2 increase of particle radius leads to a 30% increase in the clearing up intensity. In the case of smaller spheres, this dependence is stronger.<sup>15</sup> If melting and transformation of particles into droplets happen during a very short time compared to the time of complete particle destruction the influence of crystal shapes on the clearing up process is inessential.<sup>52</sup>

## Acknowledgments

This study was carried out under support from Russian Foundation for Basic Research (Grant No. 99-01-00446) and N.E. Zhukovskii Central Aero-Hydrodynamics Institute.

## References

1. 1995 *Scientific Assessment of the Atmospheric Effects of Stratospheric Aircraft*. NASA Reference Publication 138t, (Washington, DC, November 1995).
2. J. Carpentier, in: *Proceedings of International Colloquium on Impact of Aircraft Emissions upon the Atmosphere* (Paris, 1996), Vol. I, pp. 31-49.
3. U. Schumann, *Annal. Geophys.* **12**, No. 10/11, 365-384 (1994).
4. U. Schumann, in: *Pollutants from Air Traffic (Results of Atmospheric Research in 1992-1997 years)* (German Aerospace Center, 1997), pp. 1-21.
5. G.T. Amanatidis and G. Angeletty, in: *Proceedings of International Colloquium on Impact of Aircraft Emissions upon the Atmosphere* (Paris, 1996), Vol. I, pp. 51-55.
6. H.L. Wesoky and R.R. Friedl, in: *Proceedings of International Colloquium on Impact of Aircraft Emissions upon the Atmosphere* (Paris, 1996), Vol. I, pp. 57-62.
7. U. Schumann, F. Arnold, et al., in: *Proceedings of International Colloquium on Impact of Aircraft Emissions upon the Atmosphere* (Paris, 1996), Vol. I, pp. 63-68.
8. R.V. Cottingham, in: *Proceedings of International Colloquium on Impact of Aircraft Emissions upon the Atmosphere* (Paris, 1996), Vol. I, pp. 69-74.
9. P. Fabian and B. Karcher, *Phys. and Chem. of the Earth* **22**, No. 6, 1-96 (1997).
10. H.S. Johnston, *Science* **173**, No. 3996, 517-522 (1971).
11. M.N. Kogan and A.N. Kucherov, *Scientific Notes of CAHI* **29**, Nos. 1-2, 118-130 (1998).
12. A.V. Kashevarov, M.N. Kogan, A.N. Kucherov, and A.I. Stasenko, *Atmos. Oceanic Opt.* **10**, No. 12, 1568-1577 (1997).
13. A.N. Kucherov, *Atmos. Oceanic Opt.* **10**, No. 12, 1578-1587 (1997).
14. A.N. Kucherov, *Proc. SPIE* **3983**, 118-127 (1999).
15. A.N. Kucherov, in: *Proceedings of SOQUE Int. Conf. "LASERS'99"* (Quebec, Canada, 1999) (in print).
16. H.L. Hoshizaki, B. Anderson, et al., in: *CIAP (Climate Impact Assessment Program). The Stratosphere Perturbed by Propulsion Effects*, Chap. 2 (US Department of Transportation, Washington, DC, 1975).
17. B.I. Karcher, *J. Geophys. Res.* **99**, No. D7, 14509-14517 (1994).
18. T. Gerz, T. Dureck, and P. Konopka, *J. Geophys. Res.* **103**, No. D20, 25905-25913 (1998).
19. T. Gerz and F. Holzappel, *AIAA J.* **37**, No. 10, 1270-1276 (1999).
20. T. Gerz, T. Dureck, and P. Konopka, in: *Pollutants from Air Traffic* (German Aerospace Center, 1997), pp. 103-112.
21. D.C. Lewellen and W.S. Lewellen, *AIAA J.* **34**, No. 11, 2337-2345 (1996).
22. B. Karcher and P. Fabian, *Annal. Geophys.* **12**, No. 10/11, 911-919 (1994).
23. A.V. Kashevarov and A.L. Stasenko, *Scientific Notes of CAHI* **25**, Nos. 3-4, 118-130 (1994).
24. B. Karcher, *J. Geophys. Res.* **100**, No. D9, 18835-18844 (1995).

25. B. Karcher, Th. Peter, and R. Ottman, *Geophys. Res. Lett.* **22**, No. 12, 1501–1504 (1995).
26. B. Karcher, *Geophys. Res. Lett.* **23**, No. 15, 1923–1936 (1996).
27. D.C. Lewellen, W.S. Lewellen, et al., *AIAA J.* **36**, No. 8, 1439–1446 (1998).
28. R.I. Sykes and D.S. Henn, *J. Atmos. Sci.* **46**, No. 8, 1106–1118 (1989).
29. R.E. Robins and D.P. Delisi, *AIAA J.* **28**, No. 4, 661–669 (1990).
30. R.C. Miake-Lye, M. Martinez-Sanchez, R.C. Brown, and C.E. Kolb, *J. Aircraft* **30**, No. 4, 467–479 (1993).
31. T.R. Quackenbush, R.E. Teske, and A.J. Bilanin, *AIAA Paper No. 93-2944*, July 1993.
32. H. Applema, *Bulletin of American Meteorological Society* **34**, No. 1, 14–20 (1953).
33. L.T. Matveev, *Meteorol. Gidrol.*, No. 3, 3–9 (1959).
34. I.P. Mazin, *Izv. RAN, Fiz. Atmos. Okeana* **32**, No. 1, 5–18 (1996).
35. J.V. Iribarne and W.L. Godson, *Atmospheric Thermodynamics* (Reidel, Boston (USA); 1981), (Second revision edition), 259 pp.
36. A.N. Kucherov, A.P. Markelov, A.A. Semenov, A.V. Shustov, in: *Proceedings of V International Symposium on New Aviation Technology of XXI century* (Zhukovskii, 1999), Section 1.1, pp. 382–389, compact. disk, eng. lang.
37. B. Karcher, Th. Peter, and U.M. Biermann, *J. Atmos. Sci.* **53**, No. 21, 3066–3083 (1996).
38. L.E. Vasiliev, S.I. Popov, and G.P. Svishchev, *Tekhnika Vozdushnogo Flota*, Nos. 1–2, 14–17 (1994).
39. G.N. Abramovich and I.P. Girshovich, *Theory of Turbulent Jets* (Nauka, Moscow, 1984), 716 pp.
40. V.E. Zuev, Yu.D. Kopytin, and A.V. Kuzikovskii, *Nonlinear Optical Effects in Aerosols* (Nauka, Novosibirsk, 1980), 116 pp.
41. O.A. Volkovitskii, L.P. Semenov, and Yu.S. Sedunov, *Propagation of Intense Laser Radiation in Clouds* (Gidrometeoizdat, Leningrad, 1982), 312 pp.
42. V.E. Zuev, A.A. Zemlyanov, Yu.D. Kopytin, and A.V. Kuzikovskii, *High-Power Laser Radiation in Atmospheric Aerosol* (Nauka, Novosibirsk, 1984), 223 pp.
43. V.E. Zuev, A.A. Zemlyanov, and Yu.D. Kopytin, *Nonlinear Optics of the Atmosphere* (Gidrometeoizdat, Leningrad, 1989), 256 pp.
44. A.N. Kucherov, *Atmos. Oceanic Opt.* **7**, No. 10, 1379–1387 (1994).
45. A.N. Kucherov, *Kvant. Elektron.* **22**, No. 3, 253–257 (1995).
46. M. Lax, G.P. Agrawal, et al., *J. Opt. Soc. Am.* **2**, No. 5, 731–742 (1985).
47. N.N. Elkin and A.P. Napartovich, *Applied Optics of Lasers* (TsNII Atominform, Moscow, 1989).
48. A.N. Kucherov and E.V. Ustinov, *Inzh.–Fiz. Zh.* **58**, No. 41, 35–42 (1990).
49. A.N. Kucherov, *Teplofizika Vysokich Temperatur* **29**, No. 1, 144–152 (1991).
50. S.L. Glickler, *Applied Optics* **10**, No. 3, 644–650 (1971).
51. A.R. MacKenzie, M. Kulmala, A. Laaksonen, and T. V3sala, *J. Geophys. Res.* **100**, No. D6, 11275–11288 (1995).
52. A.N. Kucherov, *Intern. J. Heat Mass Transfer* (2000) (accepted to print, October 1999).
53. C.F. Bohren and D.R. Huffman, *Absorption and Scattering of Light by Small Particles* (Wiley, New York–Chichester–Brisbane–Toronto–Singapore, 1983).